Vysoké učení technické v Brně
Fakulta strojního inženýrství
Ústav konstruování

Brno University of Technology
Faculty of Mechanical Engineering
Institute of Machine and Industrial Design

PROCESSING OF THE MAGNESIUM ALLOYS BY SELECTIVE LASER MELTING METHOD

Suchý Jan, Ing.
Autor práce
Author

doc. Ing. David Paloušek, Ph.D.
Vedoucí práce
Supervisor

Disertační práce
Dissertation Thesis

Brno 2022

ABSTRACT

The topic of the presented doctoral thesis is the processing of magnesium alloy technologies of selective laser melting. The thesis elaborates in more detail the issue of corrosion resistance of the material produced in this way, relative density, and mechanical properties with emphasis on the use in biomedical applications. The main goal is to clarify the influence of process and technological parameters on the corrosion rate of the processed material.

In the first phase of the work, the relative density of the samples was examined on series of linear and volumetric samples along with the internal microstructure and mechanical properties. The second phase dealt with the influence of microstructure and surface quality on the resulting corrosion rate of the material in the simulated environment of the human body. Thanks to this, it was possible to determine the corrosion rate of the SLM processed material and to determine how it can be changed by setting of the process parameters.

During the research, it was repeatedly achieved a relative density of 99.5% with a hardness of 85 ± 6 HV, compressive strength of 416 ± 40 MPa and three-point bending strength of 212 ± 9 MPa, which are the values relatively close to human bones. At the same time, it was possible to reduce the corrosion rate of the material by almost 22% by reducing the surface roughness from the initial Ra 57.3 to Ra 34.2. However, a detailed influence of cathodic phases during the corrosion test was not tested.

This thesis provides the reader with a comprehensive overview of 3D printing of magnesium alloys along with a detailed description of the influence of process and technological parameters on the WE43 alloy production process. The thesis defines the corrosion properties of 3D printed material with a relative density of 99.5% with different surface qualities. The results further advance the knowledge in the field of biodegradable implants for medical applications.

KEYWORDS

Selective laser melting, Magnesium alloys, Homogeneous material, Microstructure, Corrosion rate

OBSAH

1   INTRODUCTION

Along with the development of additive technologies, more and more scientific efforts are focused on the processing of more demanding materials such as low-melting non-ferrous metals. This opens up scientific opportunities in application areas such as biomechanics, genetic engineering or medicine. These areas are inextricably linked to artificial implants in the human body, the purpose of which is to enable the patient to lead an almost full life, even with the loss of key organs or to help in the treatment of extensive injuries. One such injury is an extensive bone defect that current orthopaedic surgery faces [1]. In 2017, 2.7 million extensive bone defects were recorded according to the statistic from the six key-European countries by patients over the age of 50. Their treatment cost countries 37.5 billion euros in summary (reoperation, medical expenses, sick days, etc.). In addition, the prediction for 2030 counts with the next increase of 30 % due to the increased average age of humankind. The use of biodegradable implants seems to be the best solution to deal with this problem due to removing the reoperation and shorter the sick days. Biodegradable implants are also an area that has attracted humankind for more than a century and has had the considerable potential [2].

From among the biodegradable materials, magnesium and its alloys appear to be the most suitable for bone replacements. Magnesium is one of the basic building blocks of the human body and can be found naturally in human bones [3–5]. Its corrosion produces a non-toxic oxide that is excreted in the urine [6]. In addition, due to its function in the bones, it contributes to stimulating the growth of new bone tissue [7–10]. This, in conjunction with its elastic modulus, which is closer to the bone tissue more than other biodegradable materials (bone: 3–20 GPa, Mg: 41–45 GPa, Ti alloys: 110–117 GPa, stainless steels: 189–205 GPa) [6], leads to a delayed or complete prevention of implant reoperation.

However, current procedures applied to non-healing bone defects face a number of problems such as immune system rejection, insufficient space at the defect site, mechanically different properties of bones and implants, reoperations, etc. To solve these problems, bone tissue treatment is increasingly being considered directly at the defect site. However, such a treatment requires implants that take into account the extent of the injury as well as the different body structure of the patient. Applying the implant can also cause a problem with the supply of nutrients to the injured area. This can be solved by using lattice structure, which can be close in shape to the structure of the bone tissue.

The structure of human bone tissue is hierarchical. It contains three cavities and each of them has a different size in the order of tens of micrometres [11]. Each of them has a defined role in bone regeneration and mechanical integrity [12]. They also allow for nutrients to flow to the injured tissue [13]. Hierarchical bone pores can be replaced by a precisely defined lattice structure. The lattice structure can support the injured tissue at the defect site and at the same time serve as a support for cell growth at the injured site. In this way, it is possible to solve problems with the built-up area at the site of injury, cell migration, nutrient and

4

waste exchange [14, 15]. This largely minimizes the production and transmission of pathogens [16]. By designing the shape and dimensions of the structure, the elastic modulus of the material near the bone tissue can be changed, which makes it possible to eliminate the stress effects on the regenerated bone [17]. The structures are also used in other fields, mainly due to weight reduction, its absorption and acoustic properties [18, 19]. Fibre splicing, gas foaming or lyophilisation technology can be used to produce lattice structures. However, these methods provide a limited ability to control the morphology of the it [20–22], which is crucial for custom implant production. In contrast, the use of additive technologies provides the geometry that is controlled by CAD data. The "layer by layer" production method makes it possible to produce parts of complex shapes which cannot be produced by conventional methods [23].

Selective laser melting (SLM) appears to be a suitable additive method for the processing of magnesium and its alloys. This method can process a wide range of materials such as Al, Ti, CoCr, Au, Cu, Ni [24, 25]. However, the use of the SLM method requires a specific production process setting for a specific application and material. The processability of magnesium and its alloys using SLM has not yet been systematically described, although a number of publications are beginning to deal intensively with this topic. The results so far show that the material can be additively processed, although it is very difficult.

One of the biggest problems faced by parts made of magnesium alloys using the SLM method is low corrosion resistance. This can be influenced, among others, by the quality of the surface. The surface quality can be partly influenced by setting the process parameters. However, this issue has not yet been addressed in 3D-printed magnesium alloys. Therefore, this thesis will focus on describing the influence of process parameters on the surface quality of magnesium alloys and its influence on the corrosion resistance of the printed material.

2   STATE OF THE ART

2.1   Selective laser melting technology

The SLM method consists in depositing the layers of metal powder and joining them using thermal energy provided by a laser. The geometry of the printed part is controlled by CAD data, from which the laser paths for the individual layers are subsequently created. The printing itself begins with depositing the first layer on a metal plate, which should match the chemical composition of the printed material. The desired shape is hatched on the laser and the powder is welded to the build plate. The build plate with the resulting part decreases by the height of one layer, which is then deposited. By re-hatching with the laser, the molten powder is welded to the previous layer. This process is repeated until the required geometry is reached. The SLM technology is suitable for a wide range of materials such as Al, Cu, Ti, Au, Ni, Zn, Mg etc. [24, 26] and, thanks to the principle of production, it is possible to produce geometry unattainable by conventional methods [23].

The quality of the resulting parts can be controlled by a number of parameters (estimated at several tens). These may include, for example, the quality of the input material, the purity and composition of the inert atmosphere, preheating of the build plate, overpressure in the production chamber, etc. A relative density of manufactured parts close to 100 % can be achieved by a suitable combination of process parameters [27]. The parameters that have the greatest impact on the production process include laser power, scanning speed, hatch distance and the thickness of the deposited layer. These main parameters are expressed in the energy equation (2.1).

$$E = \frac{Lp}{Ls \cdot Hd \cdot Lt},$$
(2.1)

Where E is the energy density [J·mm^{-3}], Lp is the laser power [W], Ls is the laser scanning speed [mm·s^{-1}], Hd is the hatch distance [mm] and Lt is the layer thickness [mm].

The calculated energy density can be effectively used to find the areas where the printing process works permanently [28]. Subsequently, suitable ratios between the main parameters are set in the selected process area. Energy density can be expressed as linear and volumetric density. Linear energy is used for the initial considerations dealing with the weld deposition test. It serves as a primary indicator that can be used to evaluate the results of the weld deposition test. However, this value does not provide information on the production behaviour of the volumetric sample [29]. Thus, it may happen that when the same energy but different process parameters are reached, the result will be different. The energy equation associating the process parameters does not take into account the effects of other parameters such as build plate preheating or remelting of the layers. At the same time, the use of preheating and remelting can lead to a significant change in the structure of the material even outside the specified range of used energies [30, 31]. For these reasons, the energy density value is mainly used as a comparison criterion.

The parameter that can directly control the amount of input energy coming to the melting site is the laser power. A laser beam with a Gaussian profile is used as standard. By blurring it, it is possible to spread the input energy over a larger area, which can effectively reduce the depth of the weld deposition tracks if too deep. At the same time, the power of the laser has the most fundamental effect on the resulting properties of the manufactured part in comparison with other parameters [32]. The setting of the laser power, its operating mode and other properties depends on the type of laser, the type of 3D printer used and the material being processed.
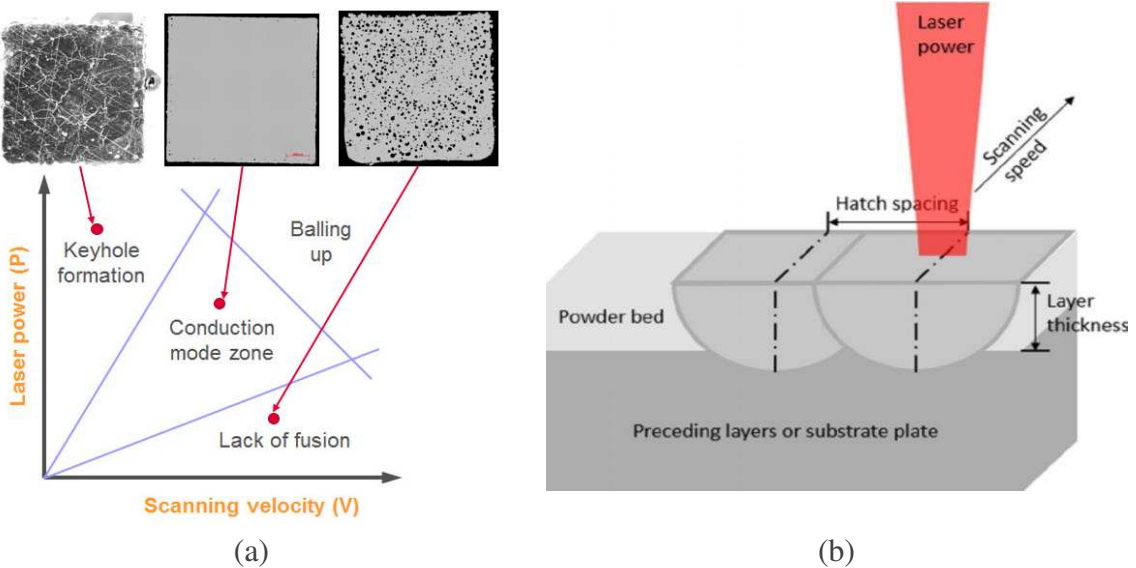

Fig 2.1 (a) Process window diagram with designation of processable and (b) definition of main process parameters [33].

The choice of scanning speed has a direct effect on the size of the melt pool at the point of impact of the laser beam. The low scanning speed leads to a large accumulation of energy at the point of impact of the beam, which increases the dimensions of the melt pool and its temperature. Since the temperature outside and at the edges of the melt pool is different [34], in this case, the melt may spatter due to unstable conditions in the melt pool [35]. The spatter droplets of melt can sinter the surrounding powder into agglomerations which disrupt the uniformity of the deposited layer and can cause porosity. Low scanning speed can also lead to a balling effect, which reduces the quality of the produced surface.

Along with the laser power, the hatch distance has the greatest effect on the production process. By bringing the weld deposition tracks closer together, they are remelted, which increases the energy densities at the melting site. This ensures stable melting of the powder even with the use of lower laser power. However, a very large hatch overlap significantly increases production time. In addition, high energy density can also lead to the formation of cavities in the material due to gas trapping [36].

The height of the layer is chosen with respect to the powder fraction used. It is most often in the range of 20–100 μm. Although the use of a lower deposited layer lengthens the production time, the benefit is an increase in the relative density of the manufactured part [37]. Increasing the height of the layer also increases the amount of material involved in the melting process. As a result, the formed weld deposition tracks are wider, which must be taken into account when choosing the hatch distances [30].

2.2   Processing of magnesium and its alloys by SLM method

The first information about attempts to process pure magnesium by the SLM method appeared in the years 2010-2011 [38–40]. The group around Ng assembled its own SLM device with a protective box, where they examined weld deposition tracks made of pure magnesium [39]. During the tests, the authors faced a constant increase in oxygen in the process chamber of the machine, which was reflected in the chemical composition of the surface of the weld depositions. Initial tests also showed a high sensitivity of the printing process to the quality of the input powder.

The follow-up test was focused on the validation of the effect of the deposited powder layer and the effect of build plate preheating [30]. The higher layer thickness reduced the amount of oxygen in the surface layer. The reason for this behaviour was probably a reduction in energy density and thus a reduction in temperature and the number of vapours at the melting site. As a result, the passivation film on the surface did not disrupt so much and oxygen could not diffuse into the material to such an extent.

The next step was a test for the production of volumetric samples, where, based on the findings from previous work, further increase in the laser power was examined [41]. However, the increase in laser power had a negative effect on the reduction in the quality of the surface to which the surrounding powder began to be fused.

The first tests on pure magnesium were quickly followed by a series of tests on selected magnesium alloys. Mg-Al-based alloys were the first, probably due to their industrial use. The initial tests were focused on the description of the process window diagram, describing the behaviour of the material when printing volumetric parts with different combinations of process parameters [28]. The microstructure of the material contained pores resembling a bloom. These were probably created by trapping the vaporized gases. At the same time, a balling effect was formed on the surface of the samples due to oxidation.

The aim of another test was to describe the behaviour of AZ91D alloy as a function of energy density and gradually increasing hatch distances [42].The energy density to 87–167 $J \cdot mm^{-3}$, the production process stabilized and the amount of evaporated material decreased. In this area, a sample with a relative density greater than 99.5 % was obtained. The low value of porosity in the material was probably caused by multiple remelting of already solidified layers of material, but the results were not confirmed by authors collective.

The inconsistency of the results between the authors gave rise to further work [32], which aimed to verify the results of the study [42]. In this work, the behaviour of weld deposition tracks was investigated when changing the laser power and the scanning speed. It has been confirmed that the laser power has a more fundamental effect on the production process than the scanning speed, both in terms of the shape of the weld depositions and the amount of evaporated material.

The results of the studies showed that increasing the laser power leads to a homogeneous material without defects. However, as the laser power increased, so did the amount of vaporized material, which prevented further testing in this direction. This problem began to be solved by designing a new inert atmosphere circuit in order to take the process emissions away from the process chamber (Fig 2.2). This concept opened up the possibility of processing magnesium and its alloys using energy densities higher than 100 $J \cdot m^{-3}$.
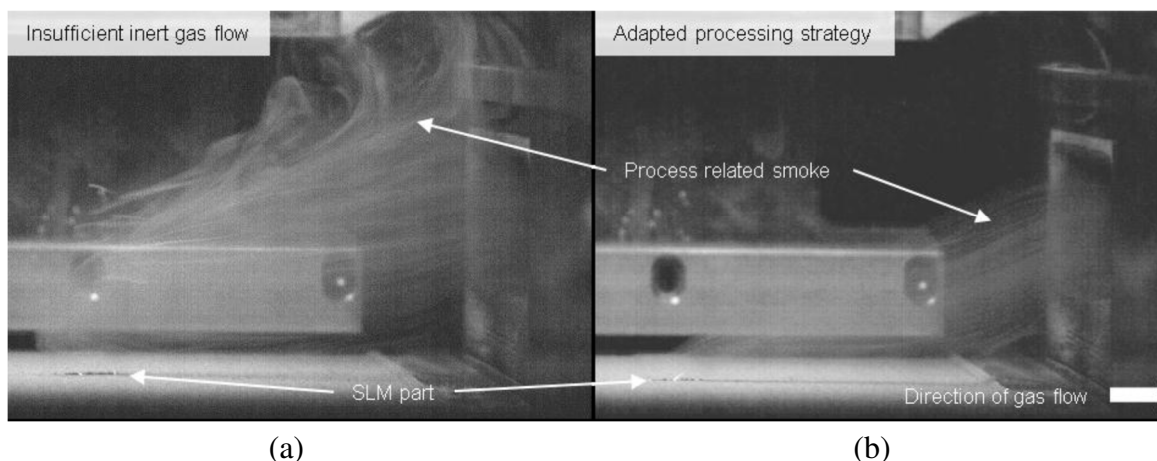

Fig 2.2 Recording of vapours during the AZ91D alloy printing process: (a) without modification of the inert atmosphere circuit; (b) with a modified inert atmosphere circuit [43].

In addition to gradually increasing the energy density, another different approach was chosen to achieve a high relative density of the samples. This approach has been briefly described here [31]. It was the printing of magnesium alloy WE43 with energy densities lower than those used for the printing of aluminium alloys. The energy was supplied to the melting site mainly via increasing the hatch overlap instead of increasing the laser power. In addition, remelting followed after each layer produced, and the resulting energy density was thus divided into two equal steps. In this way and by increasing the scanning speed to mm·s^{-1} the depth of weld depositions in the samples was limited. In this manner, a relative sample density above 99 % would be achieved with mechanical strength comparable to conventional production methods. In addition, the reduction in laser power led to a reduction in the amount of evaporated magnesium. Nevertheless, the samples contained a number of defects that negatively affected their properties.

Increasingly, reaching the relative density of samples above 99 % has led to the novice publishing activity via follow-up analyses. One of them was the description of the ultimate strength of the WE43 alloy created by SLM tensile diagram [36]. The results were related to the cast and extruded material. During the tensile test of SLM samples, a significant yield strength was observed and the SLM processed material achieved comparable properties as the extruded material. Only the elongation of the extruded material was about 40 % higher compared to the SLM material.

A more detailed analysis of the microstructure of the WE43 alloy revealed a different distribution of RE secondary phases of rare earth elements [44, 45]. Compared to the cast material, the shape of the particles was similar, but their size was significantly smaller. As a result, large cathodic phases were not formed at the same time, but the Y and Nd elements were homogeneously distributed in the material structure.

2.3 Oxidation of magnesium and its alloys

Magnesium and its alloys are subject to several types of corrosion. One of them is crystal corrosion, which occurs over a wide range of pH values. The essence of this type of corrosion is the thermodynamic instability of the metal in the environment and its effort to move to a more stable state of corrosion products through oxidation and reduction. This creates an oxide layer which, if it covers the entire metal surface, can have passivating effects. The formation of such a layer is governed by the Pilling-Bedworth molar volume rule. The chemical composition of the passivation layer depends on the chemical composition of the surrounding environment. Intergranular corrosion in magnesium alloys is not dominant, as grain boundaries usually have a higher corrosion resistance than the grains themselves [46, 47]. Magnesium alloys show a relatively good corrosion resistance in airy and dry atmospheres. The presence of joints or shapes in which water and other solutions can be retained allows for the formation of a galvanic cell, which significantly contributes to increasing the local corrosion rate.

The galvanic cell is formed at the interface of metals, which creates a large potential difference to magnesium. Galvanic corrosion can thus occur between joints (typically a magnesium sheet and steel bolts), but also within one material between its individual phases in the microstructure. Corrosion attacks the more electronegative of the pair of metals. Even in the case of galvanic corrosion, a passivation layer can form, which increases the corrosion resistance of the material. The formation of a passivation layer or possible immunity of the metal to galvanic corrosion can be predicted from the Pourbaix diagrams. The reaction describing the decomposition of the cathode by dissolving Mg to form hydrogen is given in Equations 2.2 and 2.3.

$$Mg \rightarrow Mg^{2+} + 2e^- \tag{2.2}$$

$$2H_2O + 2e^- \rightarrow H_2 + 2OH^- \tag{2.3}$$

The higher the potential voltage between the cathodic and anodic parts, the higher the reaction rate [48]. At the same time, the corrosion rate also affects environmental conditions such as temperature and solution pH. The flow of the electrolytic solution also has a very negative effect on the corrosion resistance of magnesium. Studies show that the corrosion resistance of a sample can be reduced 3-6 times in such an environment [49]. To improve the corrosion as well as mechanical properties, magnesium alloys are inoculated with alloying elements. One of the common alloying elements of magnesium alloys is aluminium. Aluminium is inexpensive, light, increases strength characteristics and reduces the anodic reaction rate of magnesium. Therefore, Mg – Al alloys do not corrode as much as magnesium alone [50]. Other alloying elements of magnesium alloys are Nd and Y. The use of these alloying elements creates intermetallic phases in the alloy, which serve as local cathodes and thus contribute to increasing the corrosion rate in the alloy [51]. On the other hand, the precipitates significantly refine and homogenize the grain. The fine grain increases the grain boundary density, which aids in the passivation of the alloy [52]. As a result, despite the higher amount of cathodic phase, it can be stated that Mg-Nd-Y alloys have the highest corrosion resistance from among the magnesium alloys [48].

As mentioned above, a higher corrosion resistance can be achieved by refining the grain. The resulting grain size corresponds to the technology by which the material is processed. By far the best results can be achieved with laser surface melting (LSM) technology[53, 54]. This technology consists in remelting the surface of the material with a laser beam, which creates a fine-grained structure on the surface of the material due to the high temperature gradient. The laser affects the material to a depth of about one millimetre. In addition, in the case of Mg-Nd-Y alloys, intermetallic phases ($Mg_{12}Nd$, $Mg_{14}Nd_2Y$, etc.) dissolve in the α-Mg solution in the area affected by the laser, thus reducing the proportion of cathodic phases and reducing the corrosion rate [55]. Similar fine grain can be achieved by using additive technologies such as selective laser melting (SLM) or electron beam melting (EBM).

The corrosion behaviour of magnesium and its alloys has been well described in the literature [56]. The corrosion rate is directly-proportionally dependent on the ambient temperature. Increasing the temperature, an ever-stronger exponential trend begins to appear, which is caused by the constant violation of the passivation layer on the surface of the material. This is mainly due to thermal expansion on the surface of the material and subsequent delamination of the already corroded layer. At temperatures above 500 °C (temperatures close to autoignition of magnesium), magnesium and its alloys are subject to catastrophic corrosion. The passivation layer is even more stressed, this time by the stress caused by the pressure of evaporated Mg.

The passivation layer of magnesium alloys is usually formed in separate regions and subsequently a continuous film is formed. The reason for this behaviour is usually the anisotropic distribution of intermetallic particles in the alloy. The passivation layer most often contains MgO and intermetallic compounds corresponding to the alloying elements of the given magnesium alloy. Mg_3N_2 compounds also appear in the passivation layer during oxidation at elevated temperatures. The reason is the exothermic reaction occurring between Mg and N at elevated temperatures; this contributes to a very poor extinguishing of the magnesium flame.

At temperatures close to the autoignition of the magnesium alloy, vapours are formed which react strongly with oxygen to form MgO. This reaction is freely expressed by equation 2.4.

$$Mg-O_{Solution} \rightarrow Mg + MgO \tag{2.4}$$

Since the temperature at the point of impact of the laser can approach temperatures above 2500 °C during the SLM process, it is necessary to process magnesium alloys under a protective inert atmosphere. As standard, magnesium alloys are printed in an argon protective atmosphere, which is not able to fully prevent of the material oxidation [57, 58]; therefore, during the production process, it is necessary to keep the oxygen value below 0.2 % by constant argon flow. However, at the same time, the question arises as to whether it is necessary to maintain a pure argon inert atmosphere or to use some other gases. Results from some publications suggest that optimizing the composition of the inert atmosphere can increase production repeatability and a range of results [59].

Successes in the field of additive processing of magnesium alloys have opened a new issue - corrosion resistance of SLM processed material. This may be different for volumetric samples and for structured material. One of the first studies dealing with the corrosion resistance of lattice structures made using SLM from WE43 magnesium alloy was reported in 2018 [60]. As the samples was chosen lattice structure and their basic mechanical pressure integrity was retained even after 28 days in a solution simulating the environment of the human body. To increase the corrosion resistance of lattice structures, their surface was modified by plasma electrolytic oxidation (PEO) [61].

When testing the corrosion rate of WE43 alloy treated by the SLM method, an increase in the degradation of the material was observed during laser processing compared to casting (Fig 2.3). The cause was the kinetics of the cathodic reaction due to the high affinity of Y and Zr for oxygen. Especially Zr formed larger agglomerations, which were the main initiators of the reaction. However, the authors themselves state that this assumption must be subjected to a more detailed test, as it goes against generally accepted claims [48, 62, 63].
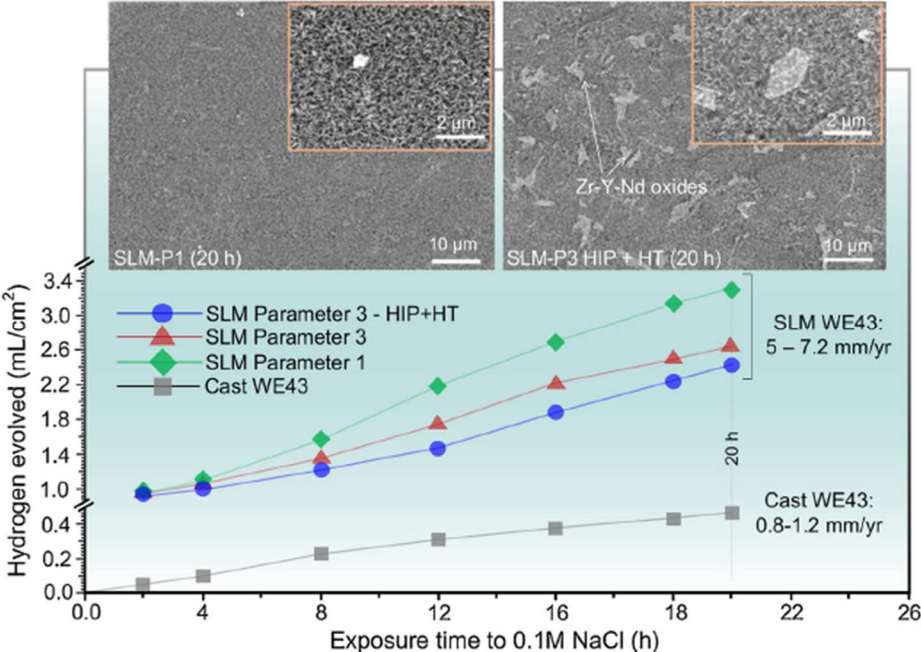

Fig 2.3 Hydrogen evolved during a corrosion test in a salt solution lasting 24 hours for different types of samples [45].

3 ANALYSIS OF THE CURRENT STATE OF THE ART

The magnesium and its alloys must be to product under an argon inert atmosphere that is more inert than nitrogen. However, the presence of the inert atmosphere does not completely prevent the oxidation of magnesium at elevated temperatures [30, 38–40, 58].]. The oxygen bound to the powder material is released during melting and begins to react violently with the surrounding material and the released vapours. During the SLM process, the material is completely melted and many studies indicate that evaporation of magnesium is a common component of this process [31, 36, 42, 64]. The magnesium vapours must be removed from the processing chamber. These vapours can defocus the laser beam. Oxidation during the production process cannot be prevented in the argon inert atmosphere without affecting the porosity of the manufactured parts. However, it can be partially controlled by selecting process parameters.

The best result for pure Mg was achieved with parameters of P = 90 W and Vs = 100 mm/s. The relative density of the sample was 95 % and hardness was 46-52 HV. The time delay during the layers printing was also tested. This showed the greatest effect on the surface quality, which improved by up to 10 μm Ra. During the production of samples, the chamber was filled with magnesium vapour, which blurred the laser beam. The best result for AZ91 was obtained with parameters P = 200 W, Hd = 90 μm, Lt = 40 μm, Vs = 333 mm/s with 99.52 % relative density [42]. Two methods of how to produce low porosity samples from WE43 were presented. In both cases, the samples reached relative densities higher than 99 % [31, 36, 65]. The first method uses process parameters P = 90 W, Vs = 800 mm/s, Hd = 45 μm, Lt = 50 μm together with the remelting of already produced layer [31]. The second method continues to use higher laser power thus remelting 5–7 layers [36, 65]. In both cases, the layers are remelted, but each time in a different way. The benefit of obtaining a higher relative density by remelting the layers was also observed by Wei et al. [42]. The relative density using the first method resulted in a porosity of more than 99 %. The second method shows a porosity better than 99.6 %. A closure of pores by isostatic hot pressing has also been tested [65]. However, the result was only the closure of large pores, the processing had almost no effect on small cavities.

The WE43 alloy was successfully processed on three machines. One is EOS M270 [65], the other is AconityMINI [36, 66]. On these machines, WE43 is processed at increased power, which generates a large amount of process emissions in the machine chamber. Due to the improved distribution of the inert atmosphere, the process emissions are more efficiently removed from the machine chamber and do not blur the laser beam and do not stick to the protective glass. Another machine that has relatively successfully processed the WE43 alloy is the SLM 125[HL] [31]. However, another processing method using a lower power and layer remelting had to be used here, as mentioned above. Due to the lower laser power, not so many process emissions that adversely affect the production process are generated in the machine chamber.

An analysis of current publications shows that the processing of magnesium and its alloys repeats the same problems caused by the physical nature of magnesium and can be solved in similar ways. However, publications indicate that process parameter settings may not be applicable when being transferred to another production machine [32]. The reason may be a different design of the printers. For older machines, the distribution of the inert atmosphere was a problem node. The next important parameters is the preheating of the build plate. Some of them allow for the build plate to be heated only up to a certain limit, which can vary significantly.

So, the main requirements for a biodegradable implant are primarily its sufficient mechanical integrity and corrosion resistance. The presented search shows that most of the produced volumetric samples contained a number of defects and disintegrated under load. Their printing was hindered by the vapour barrier of the magnesium matrix, which is a natural phenomenon of laser processing of magnesium alloys. The printing methods described so far use different combinations of process parameters and approaches, while the question remains: what is the repeatability of printing? Often, a more detailed description of the printing strategy for achieving the stated results of the relative density of the samples is missing. However, these studies show that magnesium alloys can be processed with a relative density close to 100 %. To assess which 3D printer settings achieve the best results, it is necessary to understand the influence of individual process parameters on the production process of a chosen material. With defect-free material, such as porosity, shrinkage, etc., the geometry of the implant can be adjusted to achieve human bone-like properties (compressive strength of 130-180 MPa). At the same time, such material can be used for other types of analyses, such as determination of corrosion resistance, toxicity, mutagenicity, etc.

Magnesium and its alloys face low corrosion resistance. This is due to the inability of the material to maintain a compact passivation layer. However, the results from the studies dealing with the laser processing of magnesium alloys show that corrosion of the material can be significantly slowed down. Nevertheless, information on the corrosion behaviour of magnesium alloys processed by the SLM method is still missing. Magnesium and its alloys are subject to atmospheric corrosion, the rate of which is affected by environmental influences as well as the surface quality of the material. In addition to atmospheric corrosion, galvanic corrosion also takes place in the material between the individual intermetallic phases (cathodes) and the magnesium matrix (anode). Because of this joint action, the corrosion rate of magnesium alloys reaches such high values. However, it is not known which of these corrosion methods has a dominant effect on the overall corrosion rate. The corrosion rate limit for biodegradable implants was set at 0.5 mm·year^{-1} [61]. From among the conventional methods of processing of magnesium alloys, extrusion is closest to this value, when the corrosion rate of the material reaches the values around 1.5 mm·year^{-1}. However, laser processing offers the opportunity to change the microstructure of the material and its surface quality. Volumetric samples produced so far using 3D metal printing are characterized by particularly poor surface quality. However, it should depend on the process parameters during production. Therefore, by their suitable combination, it should be possible to improve the corrosion resistance of the material.

4 GOALS OF DOCTORAL THESIS

The main goal of the presented doctoral thesis is to clarify the influence of process parameters and technological conditions on the corrosion behaviour of WE43 magnesium alloy produced by SLM method. The goal of the doctoral thesis was built on two scientific questions, which are based on the findings in Chapters 2 and 3. Working hypotheses to be tested during the work were created for these scientific questions. In order to obtain adequate answers to the scientific questions raised and to meet the main goal, it is necessary to develop the following sub-goals:

- Explain the effect of laser power and scanning speed on the geometry and continuity of weld deposition tracks.

- Explain the effect of laser power and scanning speed on the geometry and continuity of weld deposition tracks.

- Determine the effect of laser power and scanning speed on surface quality.

- Define suitable combinations of process parameters for printing volumetric samples.

- Create samples with basic mechanical strength and relative density higher than 99 %.

- Create a basic microstructural description of SLM processed material.

- Determine the corrosion rate of SLM processed material for different surface qualities.

4.1 Scientific questions

Q1. *What influences most the final value of the relative density of the WE43 magnesium alloy?*

Q2. *Is it possible to control the corrosion rate of the WE43 alloy processed by the SLM method by adjusting the process parameters?*

4.2 Hypotheses

H1. *Achieving a relative density close to 100 % is difficult in terms of the physical properties of magnesium. Its proximity to the melting point (650 °C) and the boiling point (1091 °C) causes massive evaporation of the magnesium matrix during printing, which blurs the laser beam and adversely affects the print repeatability. With a suitable combination of process parameters, the energy that melts the material could be distributed in ways other than just using the laser power* [67], *which should help to reduce vapours and stabilize the process.*
The surface quality is directly dependent on the laser power and scanning speed. A combination of these two parameters affects the energy density used to melt the metal powder. Energy density determines the fact whether the metal powder will be fully or just partially melted. Thus, a suitable value of energy density can, to some extent, prevent the surrounding powder from fusing to the surface of the printed geometry [68].

H2. *The surface of magnesium materials produced by SLM is prone to fusing of the surrounding powder. The fused powder is the main reason for the low surface quality and preventing it from fusing would significantly improve the surface of the material* [61]. *This would reduce the area that can be attacked by corrosion and significantly reduce its speed.*

5 MATERIALS AND METHODS

5.1 Achieving the reqired mechanical properties of 3D printed material WE43

As mentioned above, the PhD thesis moves the issue of biodegradable bone implants forward. In practice, these are most often checked for compressive strength and three-point bending strength, and their values should be as close as possible to the values of the bone they are intended to support. The generally stated mechanical strength of bone in compression and three-point bending for an adult reaches the order of 210 MPa and 180 MPa. It is also necessary to mention that the internal structure of the bone is porous and each of the cavities has its purpose, as already mentioned in the introduction. From this point of view, it is important to control the geometric structure in the bone and it is not possible to rely on its uncontrolled distribution. The shape and distribution of the porosity in the bone will be controlled by the shape and density of the structured lattice. Therefore, it is necessary to achieve the material with a relative density higher than 99 %, which can be declared sufficiently homogeneous.

The values against which the quality of the processed WE43 material was assessed are based on the above-mentioned values of strength and relative density. However, before the mechanical testing itself, it was first necessary to create a printing strategy for the volumetric material to achieve. Thus, it was necessary to start with linear samples and gradually switch to a volumetric variant.

In the first phase of the tests, two series of linear samples were created. The first series contained weld deposition tracks created by different combinations of laser power and scanning speeds. The shape and continuity of the tracks were monitored using a profilometer and SEM. The aim of the experiment was to find combinations of process parameters at which the weld deposition traces were stable. This allowed us to create a process map that described the behaviour of weld deposition tracks in the context of linear density of energy, laser power and scanning speed. This provided the basis for combinations of process parameters that were used as input for testing volumetric samples. The effect of laser power on the chemical composition of the weld depositions and their microhardness was also monitored on the weld deposition samples. A chemical composition analysis was performed using EDS, and microhardness was measured by HV. This test served as initial information on the mechanical properties of the processed alloy and tested the sensitivity of the resulting microstructure to a change in the parameter that supplies the energy needed for melting to the material. From the presented hypothesis of SQ1, it follows that it is the high value of laser power that is probably responsible for the formation of Mg vapours and this will have to be reduced.

After the weld depositions tests, thin walls were produced with the same combinations of process parameters. Their width corresponded to the width of one weld deposition track. The continuity and width of the thin walls were monitored and compared with the weld deposition tracks. The width of the thin walls was measured on a cut perpendicular to the build plate using an opto-digital microscope. The recorded change in width should serve as a basis for the choice of weld deposition overlap to print the volumetric samples in future tests. The smallest manufacturable width of a stable thin wall was also identified during the test. This was additional information to help the successful transition from linear samples to volumetric samples.

The next step was the transition from weld deposition to volumetric samples. To do this, several sets of cubes were made with different combinations of laser power and scanning speed from the found process window from the weld deposition test. The overlap of the hatches was based on the width of the thin walls and its value was always at least 50 % to avoid the formation of pockets with unfused powder. The value of relative density determined on selected samples was monitored by the image analysis performed on cross-sections of selected samples. A metallographic analysis also provided the information on the shape and position of defects in the material. Based on this, it was possible to evaluate the effect of changes in process parameters and gradually approach the optimal setting of the printing strategy.

Also, the hardness value was monitored on the samples. Due to its simplicity and direct link to the mechanical strength of the material, it was possible to evaluate a large number of samples and monitor the trend of its change. The value of compressive and three-point bending strength was then monitored on selected samples. This was put into the context of microstructural analysis, where the material in the cast and extruded state was compared with the 3D printed material. It was possible to identify the main differences in the individual states responsible for the different mechanical behaviour.

When processing the material, a new filtration system was gradually developed to ensure a better removal of magnesium vapours from the process chamber. After the construction and connection of the system to the inert atmosphere circuit, it was necessary to readjust the settings of the printing strategy. The reason was to achieve a higher efficiency of the laser beam by the reduction of the amount of vapour in the process chamber. The limit for completing the optimization was to reach a value of relative density close to 100 % with guaranteed repeatability of production. Thanks to these steps, it was possible to answer the first scientific question.

5.2 Corrosion behaviour of material in simulated human body environment

Another topic of the present thesis is the increase of corrosion resistance of 3D printed WE43 magnesium alloy. With conventional processing methods, the corrosion rate of the alloy ranges from 1.5 to 3.6 mm·year^{-1}, depending on the technology used. The lowest values are achieved by extrusion and, conversely, the highest ones by gravity casting. For the 3D printed material, the value of the corrosion rate in the salted simulated solution of the human body has not been determined so far. The corrosion rate requirement of biodegradable implants is 0.5 mm·year^{-1} [61]. This value can be achieved by coating the surfaces using the methods such as plasma electron oxidation (PEO), etc.

As mentioned above, there are two types of corrosion of magnesium materials - atmospheric and galvanic. Galvanic corrosion is related to the internal microstructure of the material, the distribution and size of the cathodic phases. These properties are given by the chemical composition of the alloy and its processing. Atmospheric corrosion is significantly affected by the chemical composition of the material, the properties of the corrosive environment and, last but not least, the surface quality. It was the surface quality of the 3D printed material that proved to be critically low, due to the surrounding powder fusing to the surface of the material during printing. However, the amount of fused powder should be affected by the surface temperature; therefore, it should be controllable by changing the process parameters. In this way, the corrosion rate of the 3D printed material should be reduced.

First of all, it was necessary to determine the influence of process parameters on individual types of corrosion. The surface quality of the 3D processed material, the change of which directly affects the corrosion rate, was selected as the monitored value for examining the sensitivity of atmospheric corrosion to the process parameters. For this purpose, a series of thin-walled samples was produced, the surface of which was scanned with an optical profilometer. Thin-walled samples were made by different combinations of laser power and scanning speed in correspondence with the process map dealing with the mechanical properties of the material. It was thus possible to evaluate the change in surface roughness in order to change these two main parameters.

In the following phase of the tests, the microstructure of the 3D printed material was examined and compared with the cast and extruded state. This allowed to identify differences between individual states and establish their links with individual methods of technological processing. The microstructure of the materials was monitored on metallographic cuts using light microscopy. The EDS method was used to identify the intermetallic phases and their chemical composition. By examining the microstructure of volumetric samples produced by different combinations of process parameters, the microstructure sensitivity to grain size change, chemical composition, distribution and particle shape was monitored. Based on this monitoring, it was possible to decide to what extent the galvanic corrosion can be affected by changing the process parameters.

In the last part of the thesis, an immersion test was performed to determine the corrosion rate of 3D printed material in a simulated human body environment. Several sets of samples with modified surface qualities were tested. This allowed us to determine the exact effect of surface quality on the corrosion rate of the material. In the context of the previous test of the surface quality of thin walls, it was possible to determine the effects of changing the laser power and the scanning speed on the resulting corrosion rate of the processed material.

Before and after the corrosion test, the microstructure of the material was monitored to reveal how the material corroded. The size and orientation of the grains in the material structure were monitored by EBSD. The basic chemical composition of the intermetallic phases was determined by EDS, and their distribution and shape were monitored by SEM. The exact chemical composition of the individual phases and the composition of the passivation layer after the corrosion test were determined using the XRD method. The passivation layer was also observed by SEM to determine its width and compactness. The obtained results served as a basis for a discussion over the corrosion behaviour of 3D printed material. The methodology is shown on the scheme diagram.

6   RESULTS AND DISCUSSION

6.1   Achieving the required mechanical properties of 3D printed material WE43

The first test focused on linear samples, which served as a basis for creating a strategy for printing volumetric samples. The weld depositions were produced in a wide range of laser power and scanning speeds. The aim of the test was to define the value of linear energy with which the weld depositions had a continuous track with suitable ratios between their main dimensions. The similar type of test was used in other studies [69, 70].

The measurement results were gradually divided according to several criteria. One of them was the classification according to the value of linear energy with which the weld depositions were produced. This created three areas whose boundaries, however, partially intersected precisely because of the calculated values of linear energy density. The area ($7-13$ $J \cdot mm^2$) contained continuous weld deposition tracks with a stable shape. This was also reflected in the smaller range of the dimensions of the weld deposition tracks. The weld depositions from this perspective area reached a width of $200-250$ µm, a depth of $200-300$ µm and a height of $20-40$ µm.

The width and depth of the weld depositions gradually decreased with decreasing value of linear energy density. From among the monitored process parameters, the laser power had a greater effect on the resulting shape of the weld deposition tracks. By increasing the energy above 15 $J \cdot mm^{-2}$, the magnesium material began to evaporate, forming a black mist, which has already been observed in other publications [71–73]. Laser blur due to vapours, the penetration of very deep weld depositions with root porosity and an unstable melt pool made this region unsuitable for further processing. The occurrence of vapours was possible due to the very close melting point ($545-640$ °C) and vapour (1090 °C) of magnesium alloys, and, conversely, due to the high melting points of oxides that occur on the surface of the atomized powder.

To obtain a more realistic idea of the weld deposition width when printing a volumetric sample, thin-walled samples were created in the area where the weld deposition tracks appeared to be stable. The thin walls were one weld deposition wide. However, this weld deposition was layered on top of each previous layer, thus achieving at least a partial remelting effect. This led to an increase in width. The values of the thin wall widths were subject to a large range of values due to the amount of powder fused to their surface. Nevertheless, on average, an 18 % increase in the width of the thin walls was observed compared to single weld deposition tracks. Although the width of the melt pool was increased for the thin walls, it was still subject to the same behavioural trend depending on the process parameters as the weld depositions. Due to the accumulation of heat in the material by remelting, the value of the energy density for printing a stable weld deposition (thin wall) was reduced from 7 $J \cdot mm^{-2}$ to 4.5 $J \cdot mm^{-2}$.

The design of process parameters for printing of volumetric samples was based on the defined areas of the weld deposition and thin wall test. However, printing of volumetric samples was accompanied by several problems.

One of them was a relatively large number of process emissions that appeared during the print. The used filtration system did not manage to sufficiently remove the generated vapours, which led to the accumulation of black smoke in the process chamber of the 3D printer. Many of the samples produced contained defects observable with the naked eye. Other samples, despite a porosity value above 99 %, contained cracks that resulted in low strength values during loading. Unfused powder particles and, occasionally, also lack of fusion formed at the interface of the individual printed layers, were also found in the structure of the material. The layers of material could not be fused together for two reasons. The first one was the presence of oxides, typical of RE alloys on the surface of already solidified material. Thus, the complete fusion of the new material to the previous layer occurred only when the surface layer of oxides melted. However, due to the rapid solidification, the oxide layer did not have to be melted, but only disrupted by the thermal expansion of the material. Fine particles of not fully melted oxides, broken off from the surface of the material, then formed lack of fusion in the material. The second cause could be the presence of vapours in the production chamber. Their presence could blur the laser beam; it did not have to have the required energy density when it hit the surface of the material. This hypothesis was also confirmed by the increasing rate of defects in the material in the last printed samples, when the vapours had already accumulated in the production chamber. The formation of lack of fusion probably occurred through a combination of both phenomena. The increasing value of the volume density of energy led to a reduction of the mentioned defects in the samples.

The occurrence of lack of fusion also corresponds to the behaviour of energy density. Its increase made it possible to better melt the oxidized surface of the powder and thus fuse the material more consistently together. At the same time, the value of the energy density at the point of impact of the laser was increased, despite the blurring of the laser beam. However, the increase in energy density also led to an increase in the amount of evaporated material; therefore, the process chamber was filled with black smoke more quickly. When the amount of vapour became critical, the laser beam had already been blurred to such an extent that the manufacturing process was not possible. This confirmed the assumption that the amount of evaporated magnesium had to be reduced. The parameter that most affected the manufacturing process and the presence of Mg matrix evaporation was laser power.

Porosity in the material proved to be a significant factor influencing the compressive strength. By reaching the value above 1 %, the material lost much of its strength. The measured data prove the dependence of the samples on defects in their microstructure. The best strength values were achieved in a sample with a porosity of 0.2 %, while the worst ones were achieved in a sample with a porosity of 3.5 %. The overall testing results are summarized in the final table (Tab 6.1).

Tab 6.1 Summary of results from initial measurements of hardness and compressive strength of volumetric samples.

Sample	8	13	36	41
Laser power [W]	250	250	275	275
Scanning speed [mm·s^{-1}]	450	700	450	700
Hatch distance [µm]	80	80	90	90
Porosity [%]	0.2	1.5	1.0	3.5
HV0.1	88±6	85±6	86±6	81±7
Compressive yield strength [MPa]	208	175	220	165
Ultimate commpressive strength [MPa]	395	296	386	261

The samples with the highest relative density were divided, embedded in resin and subjected to metallographic grinding. The resulting cuts were subsequently observed with an electron microscope. Samples of cast and extruded material were prepared and evaluated in the same way. By comparing the results, differences in the microstructure of the material caused by different production methods were revealed.

The cast material consisted mainly of a solid α-Mg solution and discontinuous interdendritic eutectic phases. The method of cooling the material in the cast state made it possible to achieve interdendritic phases with an average width of up to 50 µm. The dendritic phases contained Mg–Nd–Y compounds. The same compounds were observed in the extruded state. However, they did not reach such dimensions as they were disrupted by extrusion and pulverized into fine particles. The directivity corresponding to the direction of extrusion was evident on the particles. The microstructure of the 3D printed material consisted of α–Mg and interdendritic phases. Due to the rapid cooling process, the microstructure was very fine and the interdendritic phases reached an average width of only 3 µm. The microstructure of the 3D processed material was the finest of the examined states. However, the processed material contained a number of defects. Cut – outs of spherical particles were observable, at the interface of which discontinuities were formed with the remaining material; these were reflected in the overall porosity of the material. The 3D printed material contained significantly more bound oxygen in the α – Mg matrix compared to the cast and extruded state. Oxygen in the 3D printed material was bound mainly in the area of pores and welds.

For reasons of safety, machine protection and increased vapour release, the circuit in a 3D metal printer which distributed and filtered the inert atmosphere was modified. The resulting vapours had an adverse effect on printing repeatability, which was probably due to blurring of the laser beam. The resulting vapours also adhered to the protective glass of the laser, which could damage it.

In order to further reduce the formation of vapours, the process parameters for printing volumetric samples were corrected. The observations showed that the amount of vapour generated was directly proportional to the volumetric energy density for printing the samples. Therefore, the aim of the test was to reduce the number of vapours generated while maintaining the relative density of the samples above 99 %. After releasing most of the vapours from the production chamber, a sample production began to deal with uneven porosity distribution. The porosity in the part increased with increasing distance from the build plate. To achieve constant temperature conditions for each produced layer, a time delay of 100s was included between the production of individual samples in order to prevent the accumulation of thermal energy in the samples and the removal of residual vapours in the production chamber. This modification of the production process led to an even distribution of porosity in the samples and porosity of 99,48 %.

6.2 Corrosion behaviour of material in simulated human body environment

The first step in this part of the work was to determine how much the process parameters influence the microstructure of the samples. The microstructure of the samples consisted mainly of an α-Mg matrix, randomly distributed floccules rich in RE elements and eutectic phase of MgO. Its occurrence can be explained in two ways. The first one is the presence of esidual oxygen in the printer's production chamber due to the purity of the inert gas [57]. The second one was related to the release of residual oxygen from the passivation layer of the powder material. It is known that the solubility of O_2 in pure Mg is below 1 at %. Oxygen is released from the powder during the manufacturing process as part of the vapours of the magnesium matrix. However, previous findings [74], reported that the combustion reaction is not sufficiently fast to prevent magnesium-rich vapours from reaching the surface and, subsequently, diffusing into the material. The oversaturated solid Mg – $O_{solution}$ on the surface of the material precipitated according to the following equation (7.1).

$$Mg - O_{Solution} = Mg + MgO \tag{6.1}$$

Oxygen that was not burned or diffused into the surface of the material was extracted via a circuit of inert atmosphere. For this reason, the oxygen content in the chamber increased during printing and had to be corrected by a constant flow of argon atmosphere. The MgO compact film could not be formed because the material underwent repeated remelting, which divided the compact film into small particles distributed in the microstructure of the material. Directionality was not found due to the chosen meander printing strategy with a rotation of 67° on each layer. In the structure of the material, both large grains formed by the constant remelting of already solidified layers of powder and small grains around the boundaries of the weld depositions were found. The acicular shape of these grains indicates the direction of solidification from the centre of the weld deposition to its boundaries. By comparing the findings from previous tests, it can be stated that the microstructure of the samples was practically the same in terms of chemical composition, shape, size and distribution of parti-

cles for different process parameters. The only significant difference was in the relative density of the samples, the shape and the occurrence of defects.

The second step was to clarify the influence of process parameters on the surface quality of the printed material. This behaviour was observed on thin walls produced with different combinations of laser power and scanning speed. The amount of fused powder significantly reduced the surface quality of samples. It was clear from the observations that the increase in linear energy density led to an increase in the surface roughness. Again, it was confirmed that the laser power has a greater effect on the result than the scanning speed. The surface roughness Ra ranged from 34.2 to 61.3 μm. The lowest surface roughness was achieved by a combination of 100 W laser power parameters and a scanning speed of 500 mm·s^{-1}. From the given data, an equation was calculated to describe the observed surface behaviour (6.1), while its coefficient of determination was 97.68 %.

$$Y = 25.8767 + 4.062x - 0.1181x^2 \tag{6.2}$$

Findings from analyses showed a significant sensitivity of surface quality to process parameters. On the contrary, the microstructure of the material, and thus the shape and size of the cathodic phases, hardly changed with the change of process parameters. Due to the ability to significantly control the surface quality by changing the process parameters, the sensitivity of the corrosion rate to the surface quality was monitored during the immersion test.

The immersion test was performed on several sets of volumetric samples with a different surface roughness. Each set was tested for 168 h (7 days). At the beginning of the test, an electrolyte appeared in all cross-sections sets between the sample surface and the aqueous solution, which increased the corrosion rate after the first 2 hours of testing. After another 7 hours, the corrosion rate gradually decreased. The as-built set, on the other hand, showed a different behaviour. Its corrosion rate accelerated slowly. However, after 21hours of testing, the corrosion rate started to increase rapidly. This was matched by a large weight loss in the set. The average pH in the solution was 9.3, which confirmed the release of hydrogen due to alkalinization of the medium to form Mg (OH$_2$). The difference was due to the surface quality and the different passivation layer, which was different at the beginning of the test in the compared sets. While the surface of the ground sets contained predominantly MgO, because the ground samples were only in contact with dry air, only a few hours before the beginning of the immersion test. A film was formed on the surface of the samples which did not exceed 3 nm in thickness (according to the Mg–Al binary diagram) and could be easily damaged by corrosion. This corresponded to the observed rapid increase in corrosion rate in the first two hours of the test. Subsequently, the rate increase slowed down and stabilized due to the formation of a new passivation film.

In contrast, the as-built passivation film probably contained Mg (OH)$_2$ because the samples were exposed to atmospheric moisture during post-processing. The Mg (OH)$_2$ film forms a more compact layer than MgO [75]. Thus, at the beginning of the immersion test, the samples were more protected from corrosion by a more robust passivation film; therefore, the increase in corrosion rate was slower. However, these compounds are metastable and do not provide full passivation of the alloy [76]. Therefore, after overcoming the initial passivation layer, the corrosion rate began to increase rapidly in direct proportion to the surface quality of the samples. A significant increase in the corrosion rate after overcoming the initial passivation layer was caused by splitting the fused powder particles from the surface of the samples. This was reflected in the weight loss of the samples, from which the corrosion rate was calculated.

The as-built set was chosen for detailed corrosion layer testing due to the largest weight loss. The XRD test before and after immersion test revealed mainly the phases of RE elements and Mg (OH$_2$) in the samples that passed the corrosion test. A detailed analysis of the corrosion layer was performed by SEM. Regions where the samples corroded faster were identified, which led to pitting. Cracks were also found in the investigated passivation layer, which allowed for further corrosion propagation. Its EDS analysis revealed the presence of elements such as Mg, O, Y, Nd, P, Cl, Na and Ca. Alloys rich in RE elements form strong intermetallic phases with cathodic behaviour, which significantly increase their corrosion rate [51]. However, in the case of 3D printed material, they occur in much smaller sizes and thus contribute to galvanic corrosion of the material to a lesser extent. The material also contained fine needles, which were located at the boundaries of the weld depositions and corresponded to the direction of melt solidification.

7 CONCLUSION

The presented PhD thesis deals with the processing of magnesium alloy WE43 by SLM technology with the main goal to clarify the influence of process parameters on the corrosion behaviour of 3D printed material. The proposed goal was chosen with regard to the currently solved problems related to the application of biodegradable implants and it has been achieved.

The PhD thesis summarizes the most important results from previous studies dealing with the oxidation and processing of magnesium alloys using laser technologies, especially SLM technology. From the mentioned studies, hitherto undescribed places were defined and the main issues related to this topic were described. The objectives of the presented work were compiled from the above findings. To meet the main goal of the thesis, scientific questions were asked and hypotheses were developed for testing. The thesis was divided into two main parts; the results were published in several scientific articles. The thesis is a compilation of the author's published results. The first part of the thesis was devoted to the material with a relative density close to 100 % and its mechanical properties are similar to human bones.

The second part of the PhD thesis dealt with the corrosion behaviour of 3D printed material with the aim to determine what impact the parameters have on the corrosion rate of the processed material. The corrosion acting on the magnesium alloy was divided into two parts. The first one was related to the behaviour, distribution and size of the cathodic phases within the material, and operated on a galvanic principle. The second one was related to the overall surface of the material; i.e., the surface that could be subject to atmospheric corrosion. From this point of view, the tests were divided into two groups. The first one dealt with the sensitivity of the microstructure of the 3D processed material to the changes in the main process parameters while the second one examined the sensitivity of the surface quality also to the changes in the process parameters.

Thanks to the achieved findings, it is possible to formulate an answer to the first scientific question and verify or falsify the proposed hypothesis:

Q1. Magnesium evaporation during the printing process is a natural phenomenon related to the physical properties of magnesium. The biggest problem preventing the achievement of the material with a relative density close to 100 % are the newly formed magnesium vapours, which blur the laser beam and complicate the process. The evaporation process cannot be completely avoided, but it can be limited to a tolerable level.

Low energy density printing is an important factor. With its increasing value, the evaporation becomes more intense. Due to the different weight of the process parameters in the energy equation (5.3), it is necessary to increase its value by increasing the hatch overlap rather than increasing the laser power. The energy delivered to the melting site is then not concentrated in one short peak, which causes intense evaporation.

Since the magnesium alloy printing process will always generate a certain amount of vapour, it is necessary to adjust the inert atmosphere circuit so that it is sufficient to entrain vapours and not allow them to accumulate in the production chamber. This can be partially offset by a post-sample time delay, which will replace the imperfect exhaust during printing, but will significantly prolong the manufacturing process.

Q2. When an excessive amount of energy density is used, the melt pool begins to widen and affects a wider environment. This leads to the fusion of a larger amount of surrounding powder to the surface of the samples and increases the roughness of their surface. Increasing the laser power contributes significantly to this phenomenon. Conversely, increasing the scanning speed makes the melt pool smaller, which reduces the amount of affected surrounding powder and reduces surface roughness. The results are graphically summarized (**Chyba! Nenalezen zdroj odkazů.**). The corrosion rate of the material is directly proportional to the surface quality. By interpolating the curves from the graph (**Chyba! Nenalezen zdroj odkazů.**) it is possible to predict a change in the corrosion rate for the observed controllable range Ra by a value close to 30 %. The second hypothesis (H2) was also confirmed. It was observed that the better the surface quality achieved, the more effectively it reduced the corrosion rate. However, even with a surface roughness of Ra 0.11 (ground surface), a corrosion rate of 2.11 mm·year^{-1} was achieved and it is still necessary to use post-processing operations such as PEO for biodegradable implants.

The presented PhD thesis focused mainly on the flawless processing of magnesium alloy WE43 and its corrosion behaviour. The reactions of the processed alloy to the changes in the main process and technological parameters were clarified. Furthermore, the higher occurrence of the MgO phase in the 3D printed material compared to conventional processing methods was explained. A different weight of process parameters in the energy equation was proved, the modification of which reduced the amount of vapour produced during printing. The influence of the surface quality on the corrosion rate of the 3D processed material was also proportionally expressed. The corrosion rate of the material was determined for different surface qualities and the way in which the material corrodes was explained in detail.

The topic closely related to the topic of the thesis is a detailed description of the influence of cathodic phases in the microstructure of the material. However, in the thesis, this topic has not been dealt with in detail. The original estimates assumed that the corrosion rate would be reached at the level of the extruded material, which was not confirmed during testing. The difference is probably due to the significantly higher amount of oxygen bound in the 3D printed material in the metastable MgO phase and the distribution of the above - mentioned cathodic phases. Here the author sees an opportunity to build on the submitted PhD thesis.

8 BIBLIOGRAPHY

[1] VAN BAEL, S., Y. C. CHAI, S. TRUSCELLO, M. MOESEN, G. KERCKHOFS, H. VAN OOSTERWYCK, J. P. KRUTH a J. SCHROOTEN. The effect of pore geometry on the in vitro biological behavior of human periosteum-derived cells seeded on selective laser-melted Ti6Al4V bone scaffolds. *Acta Biomaterialia* [online]. 2012, **8**(7), 2824–2834. ISSN 17427061. Dostupné z: doi:10.1016/j.actbio.2012.04.001

[2] BAUMGARTNER, R. Die Osteosynthesen von Lambotte zwischen 1895 und 1907. In: *Geschichte operativer Verfahren an den Bewegungsorganen* [online]. Heidelberg: Steinkopff, 2000, s. 21–29. Dostupné z: doi:10.1007/978-3-642-57709-3_3

[3] SARIS, Nils Erik L., Eero MERVAALA, Heikki KARPPANEN, Jahangir A. KHAWAJA a Andrzei LEWENSTAM. Magnesium: An update on physiological, clinical and analytical aspects. *Clinica Chimica Acta* [online]. 2000, **294**(1–2), 1–26. ISSN 00098981. Dostupné z: doi:10.1016/S0009-8981(99)00258-2

[4] OKUMA, Toshitada. Magnesium and bone strength. *Nutrition* [online]. 2001, **17**(7–8), 679–680. ISSN 08999007. Dostupné z: doi:10.1016/S0899-9007(01)00551-2

[5] HARTWIG, Andrea. Role of magnesium in genomic stability. *Micronutrients and Genomic Stability* [online]. 2001, **475**(1–2), 113–121. ISSN 0027-5107. Dostupné z: doi:10.1016/S0027-5107(01)00074-4

[6] STAIGER, Mark P., Alexis M. PIETAK, Jerawala HUADMAI a George DIAS. Magnesium and its alloys as orthopedic biomaterials: A review. *Biomaterials* [online]. 2006, **27**(9), 1728–1734. ISSN 01429612. Dostupné z: doi:10.1016/j.biomaterials.2005.10.003

[7] REVELL, Peter A., Elsie DAMIEN, X.S. ZHANG, P. EVANS a C. Rolfe HOWLETT. The Effect of Magnesium Ions on Bone Bonding to Hydroxyapatite Coating on Titanium Alloy Implants. *Key Engineering Materials* [online]. 2004, **254**–**256**, 447–450. ISSN 1662-9795. Dostupné z: doi:10.4028/www.scientific.net/KEM.254-256.447

[8] ZREIQAT, H., C. R. HOWLETT, A. ZANNETTINO, P. EVANS, G. SCHULZE-TANZIL, C. KNABE a M. SHAKIBAEI. Mechanisms of magnesium-stimulated adhesion of osteoblastic cells to commonly used orthopaedic implants. *Journal of Biomedical Materials Research* [online]. 2002, **62**(2), 175–184. ISSN 00219304. Dostupné z: doi:10.1002/jbm.10270

[9] YAMASAKI, Y., Y. YOSHIDA, M. OKAZAKI, A. SHIMAZU, T. KUBO, Y. AKAGAWA a T. UCHIDA. Action of FGMgCO3Ap-collagen composite in promoting bone formation. *Biomaterials* [online]. 2003, **24**(27), 4913–4920. ISSN 01429612. Dostupné z: doi:10.1016/S0142-9612(03)00414-9

[10] LEVOROVA, Jitka, Jaroslava DUSKOVA, Milan DRAHOS, Radka VRBOVA, D VOJTECH, Jiri KUBASEK, Martin BARTOS, Lenka DUGOVA, Dan ULMANN a Rene FOLTAN. In vivo study on biodegradable magnesium alloys: Bone healing around WE43 screws. *Journal of Biomaterials Applications* [online]. 2018, **32**(7), 886–895. ISSN 0885-3282. Dostupné z: doi:10.1177/0885328217743321

[11] MANAKARI, Vyasaraj, Gururaj PARANDE a Manoj GUPTA. *Selective Laser Melting of Magnesium and Magnesium Alloy Powders: A Review* [online]. 2016. ISBN 6565166358. Dostupné z: doi:10.3390/met7010002

[12] SIETSEMA, W. K. Animal models of cortical porosity. *Bone* [online]. 1995, **17**(4 SUPPL.), 297–305. ISSN 87563282. Dostupné z: doi:10.1016/8756-3282(95)00307-Y

[13] ZARDIACKAS, Lyle D., Douglas E. PARSELL, Lance D. DILLON, Darrell W. MITCHELL, Laura A. NUNNERY a Robert POGGIE. Structure, metallurgy, and mechanical properties of a porous tantalum foam. *Journal of Biomedical Materials Research* [online]. 2001, **58**(2), 180–187. ISSN 00219304. Dostupné z: doi:10.1002/1097-4636(2001)58:2<180::AID-JBM1005>3.0.CO;2-5

[14] HOLLISTER, Scott J. Scaffold design and manufacturing: From concept to clinic. *Advanced Materials* [online]. 2009, **21**(32–33), 3330–3342. ISSN 09359648. Dostupné z: doi:10.1002/adma.200802977

[15] HUTMACHER, Dietmar Werner, Jan Thorsten SCHANTZ, Christofer Xu Fu LAM, Kim Cheng TAN a Thiam Chye LIM. State of the art and future directions of scaffold-based bone engineering from a biomaterials perspective. *Journal of Tissue Engineering and Regenerative Medicine* [online]. 2007, **1**(June), 245–260. ISSN 15654753. Dostupné z: doi:10.1002/term

[16] HUTMACHER, Dietmar W. Scaffolds in tissue engineering bone and cartilage. *The Biomaterials: Silver Jubilee Compendium* [online]. 2000, **21**, 2529–2543. Dostupné z: doi:10.1016/B978-008045154-1.50021-6

[17] LEFEBVRE, Louis Philippe, John BANHART a David C. DUNAND. Porous metals and metallic foams: Current status and recent developments. *Advanced Engineering Materials* [online]. 2008, **10**(9), 775–787. ISSN 14381656. Dostupné z: doi:10.1002/adem.200800241

[18] NAKAJIMA, Hideo. Fabrication, properties and application of porous metals with directional pores. *Progress in Materials Science* [online]. 2007, **52**(7), 1091–1173. ISSN 00796425. Dostupné z: doi:10.1016/j.pmatsci.2006.09.001

[19] EVANS, A. G., J. W. HUTCHINSON, N. A. FLECK, M. F. ASHBY a H. N.G. WADLEY. The topological design of multifunctional cellular metals. *Progress in Materials Science* [online]. 2001, **46**(3–4), 309–327. ISSN 00796425. Dostupné z: doi:10.1016/S0079-6425(00)00016-5

[20] ALVAREZ, Kelly a Hideo NAKAJIMA. Metallic scaffolds for bone regeneration. *Materials* [online]. 2009, **2**(3), 790–832. ISSN 19961944. Dostupné z: doi:10.3390/ma2030790

[21]   HOLLISTER, Scott J. Porous scaffold design for tissue engineering. *Nature Materials* [online]. 2005, **4**(7), 518–524. ISSN 1476-4660. Dostupné z: doi:10.1038/nmat1421

[22]   SACHLOS, E., J. T. CZERNUSZKA, S. GOGOLEWSKI a M. DALBY. Making tissue engineering scaffolds work. Review on the application ofsolid freeform fabrication technology to the production of tissue engineeringscaffolds. *European Cells and Materials* [online]. 2003, **5**, 29–40. ISSN 14732262. Dostupné z: doi:10.22203/eCM.v005a03

[23]   RIZA, S.H., S.H. MASOOD a C. WEN. Laser-Assisted Additive Manufacturing for Metallic Biomedical Scaffolds. In: *Comprehensive Materials Processing* [online]. B.m.: Elsevier, 2014 [vid. 2018-05-25], s. 285–301. ISBN 9780080965338. Dostupné z: doi:10.1016/B978-0-08-096532-1.01017-7

[24]   YAP, C. Y., C. K. CHUA, Z. L. DONG, Z. H. LIU, D. Q. ZHANG, L. E. LOH a S. L. SING. Review of selective laser melting: Materials and applications. *Applied Physics Reviews* [online]. 2015, **2**(4). ISSN 19319401. Dostupné z: doi:10.1063/1.4935926

[25]   GU, D D, W MEINERS, K WISSENBACH a R POPRAWE. Laser additive manufacturing of metallic components: materials, processes and mechanisms. *International Materials Reviews* [online]. 2012, **57**(3), 133–164. ISSN 0950-6608. Dostupné z: doi:10.1179/1743280411Y.0000000014

[26]   GU, Dongdong. *Laser Additive Manufacturing of High-Performance Materials* [online]. Berlin, Heidelberg: Springer Berlin Heidelberg, 2015. ISBN 978-3-662-46088-7. Dostupné z: doi:10.1007/978-3-662-46089-4

[27]   SUCHY, Jan, Libor PANTELEJEV, David PALOUSEK, Daniel KOUTNY a Jozef KAISER. Processing of AlSi9Cu3 alloy by selective laser melting. *Powder Metallurgy* [online]. 2020, **63**(3), 197–211. ISSN 17432901. Dostupné z: doi:10.1080/00325899.2020.1792675

[28]   ZHANG, Baicheng, Hanlin LIAO a Christian CODDET. Effects of processing parameters on properties of selective laser melting Mg–9%Al powder mixture. *Materials & Design* [online]. 2012, **34**, 753–758. ISSN 02613069. Dostupné z: doi:10.1016/j.matdes.2011.06.061

[29]   PAWLAK, Andrzej, Maria ROSIENKIEWICZ a Edward CHLEBUS. Design of experiments approach in AZ31 powder selective laser melting process optimization. *Archives of Civil and Mechanical Engineering* [online]. 2017, **17**(1), 9–18. ISSN 16449665. Dostupné z: doi:10.1016/j.acme.2016.07.007

[30]   SAVALANI, Monica Mahesh a Jorge Martinez PIZARRO. Effect of preheat and layer thickness on selective laser melting (SLM) of magnesium. *Rapid Prototyping Journal* [online]. 2016, **22**(1), 115–122. ISSN 1355-2546. Dostupné z: doi:10.1108/RPJ-07-2013-0076

[31]   TANDON, Rajiv, Todd PALMER, Matthias GIESEKE a Christian NOELKE. Additive Manufacturing of Magnesium Alloy Powders: Investigations Into Process Development Using Elektron®MAP+43 Via Laser Powder Bed Fusion and Directed Energy Deposition. *Euro PM2016*. 2016, **91**, 4–9.

[32]   SCHMID, Dominik, Johanna RENZA, Michael F. ZAEH a Johannes GLASSCHROEDER. Process influences on laser-beam melting of the magnesium alloy AZ91. *Physics Procedia* [online]. 2016, **83**, 927–936. ISSN 18753892. Dostupné z: doi:10.1016/j.phpro.2016.08.097

[33]   HASMUNI, Noreriyanti, Mustaffa IBRAHIM, Azli Amin RAUS, Md Saidin WAHAB a Khairu KAMARUDIN. Porosity effects of AlSi10mg parts produced by selective laser melting. *Journal of Mechanical Engineering*. 2018, **5**(Specialissue4), 246–255. ISSN 2550164X.

[34]   WEI, Kaiwen, Zemin WANG a Xiaoyan ZENG. Influence of element vaporization on formability, composition, microstructure, and mechanical performance of the selective laser melted Mg-Zn-Zr components. *Materials Letters* [online]. 2015, **156**, 187–190. ISSN 18734979. Dostupné z: doi:10.1016/j.matlet.2015.05.074

[35]   LOUVIS, Eleftherios, Peter FOX a Christopher J. SUTCLIFFE. Selective laser melting of aluminium components. *Journal of Materials Processing Technology* [online]. 2011, **211**(2), 275–284. ISSN 09240136. Dostupné z: doi:10.1016/j.jmatprotec.2010.09.019

[36]   ZUMDICK, Naemi A., Lucas JAUER, Lisa C. KERSTING, Tatiana N. KUTZ, Johannes H. SCHLEIFENBAUM a Daniela ZANDER. Additive manufactured WE43 magnesium: A comparative study of the microstructure and mechanical properties with those of powder extruded and as-cast WE43. *Materials Characterization* [online]. 2019, **147**(August 2018), 384–397. ISSN 10445803. Dostupné z: doi:10.1016/j.matchar.2018.11.011

[37]   SAVALANI, M.M., L. HAO, P.M. DICKENS, Y. ZHANG, K.E. TANNER a R.A. HARRIS. The effects and interactions of fabrication parameters on the properties of selective laser sintered hydroxyapatite polyamide composite biomaterials. *Rapid Prototyping Journal* [online]. 2012, **18**(1), 16–27. ISSN 1355-2546. Dostupné z: doi:10.1108/13552541211193467

[38]   NG, C. C., M. M. SAVALANI, H. C. MAN a I. GIBSON. Layer manufacturing of magnesium and its alloy structures for future applications. *Virtual and Physical Prototyping* [online]. 2010, **5**(1), 13–19. ISSN 17452759. Dostupné z: doi:10.1080/17452751003718629

[39]   CHUNG NG, Chi, Monica SAVALANI a Hau CHUNG MAN. Fabrication of magnesium using selective laser melting technique. *Rapid Prototyping Journal* [online]. 2011, **17**(6), 479–490. ISSN 1355-2546. Dostupné z: doi:10.1108/13552541111184206

[40]   NG, C. C., M. M. SAVALANI, M. L. LAU a H. C. MAN. Microstructure and mechanical properties of selective laser melted magnesium. *Applied Surface Science* [online]. 2011, **257**(17), 7447–7454. ISSN 01694332. Dostupné z: doi:10.1016/j.apsusc.2011.03.004

32

[41]   HU, Dong, Yong WANG, Dingfei ZHANG, Liang HAO, Junjie JIANG, Zhonghua LI a Yitao CHEN. Experimental Investigation on Selective Laser Melting of Bulk Net-Shape Pure Magnesium. *Materials and Manufacturing Processes* [online]. 2015, **30**(11), 1298–1304. ISSN 15322475. Dostupné z: doi:10.1080/10426914.2015.1025963

[42]   WEI, Kaiwen, Ming GAO, Zemin WANG a Xiaoyan ZENG. Effect of energy input on formability, microstructure and mechanical properties of selective laser melted AZ91D magnesium alloy. *Materials Science and Engineering A* [online]. 2014, **611**, 212–222. ISSN 09215093. Dostupné z: doi:10.1016/j.msea.2014.05.092

[43]   JAUER, Lucas, Wilhelm MEINERS, Simon VERVOORT, Christoph GAYER, Naemi A. ZUMDICK a Daniela ZANDER. Selective laser melting of magnesium alloys. In: *World PM 2016 Congress and Exhibition*. B.m.: European Powder Metallurgy Association (EPMA), 2016. ISBN 9781899072484.

[44]   BÄR, Florian, Leopold BERGER, Lucas JAUER, Güven KURTULDU, Robin SCHÄUBLIN, Johannes H. SCHLEIFENBAUM a Jörg F. LÖFFLER. Laser additive manufacturing of biodegradable magnesium alloy WE43: A detailed microstructure analysis. *Acta Biomaterialia* [online]. 2019, (xxxx). ISSN 18787568. Dostupné z: doi:10.1016/j.actbio.2019.05.056

[45]   ESMAILY, M., Z. ZENG, A. N. MORTAZAVI, A. GULLINO, S. CHOUDHARY, T. DERRA, F. BENN, F. D'ELIA, M. MÜTHER, S. THOMAS, A. HUANG, A. ALLANORE, A. KOPP a N. BIRBILIS. A detailed microstructural and corrosion analysis of magnesium alloy WE43 manufactured by selective laser melting. *Additive Manufacturing* [online]. 2020, **35**(April), 101321. ISSN 22148604. Dostupné z: doi:10.1016/j.addma.2020.101321

[46]   GHALI, Edward, Wolfgang DIETZEL a Karl Ulrich KAINER. Testing of general and localized corrosion of magnesium alloys: A critical review. *Journal of Materials Engineering and Performance* [online]. 2004, **13**(5), 517–529. ISSN 10599495. Dostupné z: doi:10.1361/10599490420665

[47]   SONG, Guang Ling a Andrej ATRENS. Corrosion mechanisms of magnesium alloys. *Advanced Engineering Materials* [online]. 1999, **1**(1), 11–33. ISSN 14381656. Dostupné z: doi:10.1002/(SICI)1527-2648(199909)1:1<11::AID-ADEM11>3.0.CO;2-N

[48]   GUSIEVA, K., C. H. J. DAVIES, J. R. SCULLY a N. BIRBILIS. Corrosion of magnesium alloys: the role of alloying. *International Materials Reviews* [online]. 2015, **60**(3), 169–194. ISSN 0950-6608. Dostupné z: doi:10.1179/1743280414Y.0000000046

[49]   LI, X P, K M O DONNELL a T B SERCOMBE. Selective laser melting of Al-12Si alloy : Enhanced densification via powder drying [online]. 2016, **10**, 10–14. Dostupné z: doi:10.1016/j.addma.2016.01.003

[50]   POLMEAR, I J, IJP a I J POLMEAR. Light Alloys. In: I J POLMEAR, ed. *Light Alloys (Fourth Edition)* [online]. Fourth Edi. Oxford: Butterworth-Heinemann, 2005, s. 413. ISBN 978-0-7506-6371-7. Dostupné z: doi:https://doi.org/10.1016/B978-075066371-7/50006-2

[51]   SÜDHOLZ, A. D., N. T. KIRKLAND, R. G. BUCHHEIT a N. BIRBILIS. Electrochemical Properties of Intermetallic Phases and Common Impurity Elements in Magnesium Alloys. *Electrochemical and Solid-State Letters* [online]. 2011, **14**(2), C5. ISSN 10990062. Dostupné z: doi:10.1149/1.3523229

[52]   RALSTON, K. D., G. WILLIAMS a N. BIRBILIS. Effect of pH on the Grain Size Dependence of Magnesium Corrosion. *CORROSION* [online]. 2012, **68**(6), 507–517. ISSN 0010-9312. Dostupné z: doi:10.5006/i0010-9312-68-6-507

[53]   SINGH, Ashish a Sandip P. HARIMKAR. Laser surface engineering of magnesium alloys: A review. *Jom* [online]. 2012, **64**(6), 716–733. ISSN 10474838. Dostupné z: doi:10.1007/s11837-012-0340-2

[54]   GUAN, Y. C., W. ZHOU, H. Y. ZHENG a Z. L. LI. Solidification microstructure of AZ91D Mg alloy after laser surface melting. *Applied Physics A: Materials Science and Processing* [online]. 2010, **101**(2), 339–344. ISSN 09478396. Dostupné z: doi:10.1007/s00339-010-5880-0

[55]   LIU, Cancan, Qingbiao LI, Jun LIANG, Jiansong ZHOU a Lingqian WANG. Microstructure and corrosion behaviour of laser surface melting treated WE43 magnesium alloy. *RSC Adv.* [online]. 2016, **6**(36), 30642–30651. ISSN 2046-2069. Dostupné z: doi:10.1039/C5RA27010C

[56]   CZERWINSKI, F. The oxidation behaviour of an AZ91D magnesium alloy at high temperatures [online]. 2002, **50**, 2639–2654. Dostupné z: https://www.sciencedirect.com/science/article/pii/S1359645402000940

[57]   SALEHI, Mojtaba, Saeed MALEKSAEEDI, Hamidreza FARNOUSH, Mui Ling Sharon NAI, Ganesh Kumar MEENASHISUNDARAM a Manoj GUPTA. An investigation into interaction between magnesium powder and Ar gas: Implications for selective laser melting of magnesium. *Powder Technology* [online]. 2018, **333**, 252–261. ISSN 1873328X. Dostupné z: doi:10.1016/j.powtec.2018.04.026

[58]   ZONG, Fujian, Chunzhan MENG, Zhiming GUO, Feng JI, Hongdi XIAO, Xijian ZHANG, Jin MA a Honglei MA. Synthesis and characterization of magnesium nitride powder formed by Mg direct reaction with N2. *Journal of Alloys and Compounds* [online]. 2010, **508**(1), 172–176. ISSN 09258388. Dostupné z: doi:10.1016/j.jallcom.2010.07.224

[59]   ABEL, Arvid, Yvonne WESSARGES, Stefan JULMI, Christian HOFF, Jörg HERMSDORF, Christian KLOSE, Hans Jürgen MAIER, Stefan KAIERLE a Ludger OVERMEYER. Laser powder bed fusion of WE43 in hydrogen-argon-gas atmosphere. *Procedia CIRP* [online]. 2020, **94**, 21–24. ISSN 22128271. Dostupné z: doi:10.1016/j.procir.2020.09.005

[60]   LI, Y., J. ZHOU, P. PAVANRAM, M. A. LEEFLANG, L. I. FOCKAERT, B. POURAN, N. TÜMER, K. U. SCHRÖDER, J. M.C. MOL, H. WEINANS, H. JAHR a A. A. ZADPOOR. Additively manufactured biodegradable porous magnesium. *Acta Biomaterialia* [online]. 2018, **67**, 378–392. ISSN 18787568. Dostupné z: doi:10.1016/j.actbio.2017.12.008

[61]   KOPP, Alexander, Thomas DERRA, Max MÜTHER, Lucas JAUER, Johannes H. SCHLEIFENBAUM, Maximilian VOSHAGE, Ole JUNG, Ralf SMEETS a Nadja KRÖGER. Influence of design and postprocessing parameters on the degradation behavior and mechanical properties of additively manufactured magnesium scaffolds. *Acta Biomaterialia* [online]. 2019, (xxxx). ISSN 18787568. Dostupné z: doi:10.1016/j.actbio.2019.04.012

[62]   SUDHOLZ, A. D., K. GUSIEVA, X. B. CHEN, B. C. MUDDLE, M. A. GIBSON a N. BIRBILIS. Electrochemical behaviour and corrosion of Mg-Y alloys. *Corrosion Science* [online]. 2011, **53**(6), 2277–2282. ISSN 0010938X. Dostupné z: doi:10.1016/j.corsci.2011.03.010

[63]   DAVENPORT, Alison J., Cristiano PADOVANI, Brian J. CONNOLLY, Nicholas P.C. STEVENS, Thomas A.W. BEALE, Amela GROSO a Marco STAMPANONI. Synchrotron X-ray microtomography study of the role of y in corrosion of magnesium alloy WE43. *Electrochemical and Solid-State Letters* [online]. 2007, **10**(2), 4–8. ISSN 10990062. Dostupné z: doi:10.1149/1.2400727

[64]   JAUER, L, B JÜLICH, M VOSHAGE a W MEINERS. Selective Laser Melting of magnesium alloys. 2015, **30**(page 1), 824682.

[65]   GANGIREDDY, Sindhura, Bharat GWALANI, Kaimiao LIU, Eric J. FAIERSON a Rajiv S. MISHRA. Microstructure and mechanical behavior of an additive manufactured (AM) WE43-Mg alloy. *Additive Manufacturing* [online]. 2019, **26**(September 2018), 53–64. ISSN 22148604. Dostupné z: doi:10.1016/j.addma.2018.12.015

[66]   LI, Y, J ZHOU, P PAVANRAM, M A LEEFLANG, L I FOCKAERT, B POURAN, N TÜMER, K SCHRÖDER, J M C MOL, H WEINANS, H JAHR a A A ZADPOOR. Additively manufactured biodegradable porous magnesium. *Acta Biomaterialia* [online]. 2018, **67**, 378–392. Dostupné z: doi:10.1016/j.actbio.2017.12.008

[67]   SCIPIONI BERTOLI, Umberto, Alexander J. WOLFER, Manyalibo J. MATTHEWS, Jean Pierre R. DELPLANQUE a Julie M. SCHOENUNG. On the limitations of Volumetric Energy Density as a design parameter for Selective Laser Melting. *Materials and Design* [online]. 2017, **113**, 331–340. ISSN 18734197. Dostupné z: doi:10.1016/j.matdes.2016.10.037

[68]   KRÓL, M. a T. TASKI. Surface quality research for selective laser melting of TI-6AL-4V alloy. *Archives of Metallurgy and Materials* [online]. 2016, **61**(3), 945–950. ISSN 17333490. Dostupné z: doi:10.1515/amm-2016-0213

[69]   GUO, Yueling, Lina JIA, Bin KONG, Na WANG a Hu ZHANG. Single track and single layer formation in selective laser melting of niobium solid solution alloy. *Chinese Journal of Aeronautics* [online]. 2018, **31**(4), 860–866. ISSN 10009361. Dostupné z: doi:10.1016/j.cja.2017.08.019

[70]   KEMPEN, K., W. Verheecke L. THIJS , E. YASA, M. BADROSSAMAY a Department J.-P. KRUTH. Process Optimization and Microstructural Analysis for Selective Laser Melting of AlSi10Mg. In: . 2011, s. 484–495.

[71]   CZERWINSKI, Frank. Controlling the ignition and flammability of magnesium for aerospace applications. *Corrosion Science* [online]. 2014, **86**, 1–16. ISSN 0010938X. Dostupné z: doi:10.1016/j.corsci.2014.04.047

[72]   TEKUMALLA, Sravya a Manoj GUPTA. An insight into ignition factors and mechanisms of magnesium based materials: A review. *Materials and Design* [online]. 2017, **113**, 84–98. ISSN 18734197. Dostupné z: doi:10.1016/j.matdes.2016.09.103

[73]   ZHAN, Xiaohong, Jicheng CHEN, Junjie LIU, Yanhong WEI, Junjie ZHOU a Yao MENG. Microstructure and magnesium burning loss behavior of AA6061 electron beam welding joints. *Materials and Design* [online]. 2016, **99**, 449–458. ISSN 18734197. Dostupné z: doi:10.1016/j.matdes.2016.03.058

[74]   DREIZIN, Edward L., Charles H. BERMAN a Edward P. VICENZI. Condensed-phase modifications in magnesium particle combustion in air. *Combustion and Flame* [online]. 2000, **122**(1–2), 30–42. ISSN 00102180. Dostupné z: doi:10.1016/S0010-2180(00)00101-2

[75]   TAHERI, M. a J. R. KISH. Nature of Surface Film Formed on Mg Exposed to 1 M NaOH. *Journal of The Electrochemical Society* [online]. 2013, **160**(1), C36–C41. ISSN 0013-4651. Dostupné z: doi:10.1149/2.018302jes

[76]   LI, Zijian, Xunan GU, Siquan LOU a Yufeng ZHENG. The development of binary Mg-Ca alloys for use as biodegradable materials within bone. *Biomaterials* [online]. 2008, **29**(10), 1329–1344. ISSN 01429612. Dostupné z: doi:10.1016/j.biomaterials.2007.12.021

9 LIST OF FIGURES AND TABLES

List of figures

Seznam tabulek